Fabrication and measured quality of the MMT primary mirror

H. M. Martin, R. G. Allen, J. R. P. Angel, J. H. Burge, W. B. Davison, S. T. DeRigne, L. R. Dettmann, D. A. Ketelsen, W. C. Kittrell, S. M. Miller, P. A. Strittmatter and S. C. West

Steward Observatory, University of Arizona, Tucson, AZ 85721

ABSTRACT

The primary mirror for the Multiple Mirror Telescope Conversion is the first 6.5 m honeycomb sandwich mirror cast and polished by the Steward Observatory Mirror Lab. We describe the optical fabrication and testing of the f/1.25 paraboloid, and present the final measurements of figure accuracy and inferred image quality. Figuring was performed with a 1.2 m stressed lap–which bends under active control to match the local curvature of the optical surface–and a variety of small passive tools. The mirror was pressurized to compensate for polishing loads and thereby eliminate print-through of the honeycomb structure. The net result is a smoother surface on scales of 5-20 cm than has been achieved on previous honeycomb sandwich mirrors. The figure was measured with IR and visible interferometers, using refractive null correctors to compensate 810 microns of aspheric departure. The final measurements were used to calculate synthetic stellar images in a variety of seeing conditions.

Keywords: telescopes, optical fabrication, optical testing, aspheres

1. INTRODUCTION

The Multiple Mirror Telescope on Mt. Hopkins in southern Arizona is being converted to a single-mirror telescope, with a 6.5 m primary mirror replacing its six 1.8 m mirrors.[1] The single primary provides several advantages, especially a doubling of the collecting area by use of a filled aperture, and a 15-fold increase in field of view to 1°. Because the existing enclosure and much of the telescope structure can be used with minor modification, the enhanced performance is achieved economically.

The 6.5 m mirror, shown in Figure 1, is a honeycomb sandwich, the first of its size cast at the Steward Observatory Mirror Lab.[2] The concave front shell and flat back plate are each about 27 mm thick, and these are separated by 12 mm ribs in a hexagonal pattern with 192 mm spacing. The overall thickness is 0.71 m at the edge. In order to make the new telescope fit in the existing MMT building, this mirror is considerably faster at f/1.25 than most large mirrors. The short focal length is an advantage as well as a necessity, making the structure stiff and giving a large plate scale (1° in 0.6 m) at the f/5 Cassegrain focus without requiring an excessively large secondary. For these reasons, and because of the compact and economical enclosure, a number of other projects using honeycomb sandwich mirrors have adopted equal or faster focal ratios.[3,4]

Such fast mirrors present the challenge of polishing the extremely aspheric surface, and the Mirror Lab's polishing system is designed for that purpose. Most lapping operations are performed with a stressed lap that is relatively large (1.2 m) and stiff, and maintains fit through continuous active shape changes.[5-7] Previous experience with the stressed lap included a 1.8 m f/1 primary and three 3.5 m primaries of f/1.5-f/1.75, all honeycomb sandwich mirrors, figured to about 20 nm rms surface and operating successfully in telescopes (Vatican Advanced Technology, Air Force SOR, ARC, and WIYN). The MMT primary is a step up in size and asphericity. The accuracy requirement is stringent also, corresponding to a seeing-limited image size of 0.092 arcsecond FWHM and a scattering loss due to small-scale structure of 1.5% (both at 500 nm wavelength).

Part of the SPIE Conference on Advanced Technology Optical/IR Telescopes VI • Kona, Hawaii • March 1998
SPIE Vol. 3352 • 0277-786X/98/$10.00

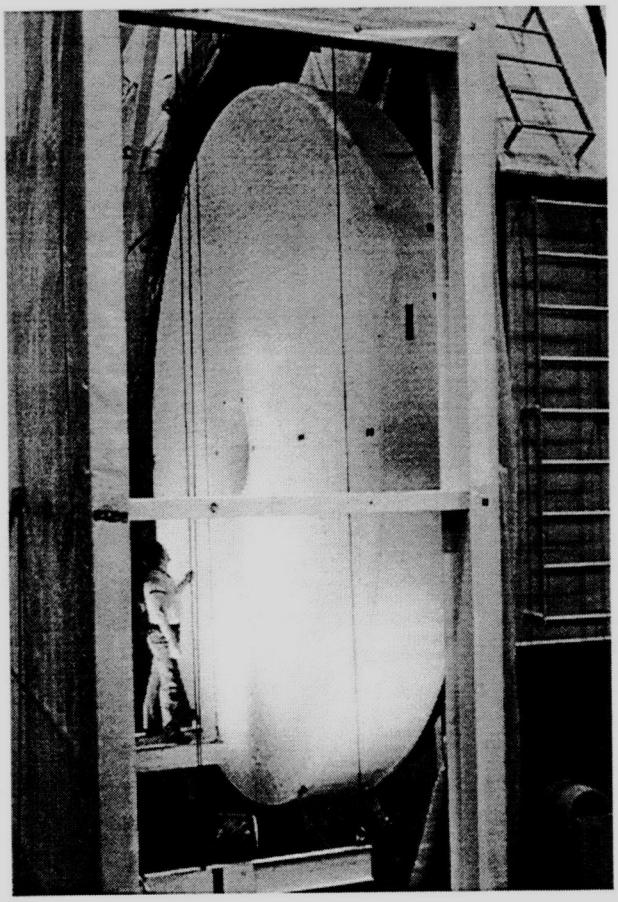

Figure 1. MMT primary mirror, viewed from the back, on its turning frame.

2. ACCURACY REQUIREMENTS

The optical error budget for the MMT Conversion is given in terms of the wavefront structure function, often used to characterize the wavefront perturbed by the atmosphere. The structure function D_φ is the mean square phase difference between pairs of points in the aperture as a function of the separation r between those points. Knowledge of the structure function fully determines the long-exposure optical transfer function and point-spread function. Since our goal is to ensure that the telescope does not significantly degrade the best seeing-limited wavefront, we adopt the form of the ideal atmospheric structure function,

$$D_\varphi(r) = 7.12\left(\frac{r\theta}{\lambda}\right)^{5/3} \text{rad}^2, \qquad (1)$$

with each component of the error budget allocated an image size θ defined as the full width at half maximum. The structure functions of the components add linearly to give the combined structure function.

The goal for the primary mirror surface is an error corresponding to seeing of 0.092 arcsecond FWHM at $\lambda = 500$ nm . The ideal atmospheric structure function approaches zero toward small separations. In order to soften this requirement of infinite smoothness, the mirror surface structure function is allowed to approach a constant for small spacings, corresponding to small-scale structure that scatters some fraction of the light over wide angles. The allowed loss for the MMT primary is 1.5% at 500 nm. At large separations, the atmospheric wavefront error is dominated by tilt, which varies sufficiently slowly that it will be removed by autoguiding. For this reason, and the fact that tilt is ignored in lab measurements of the primary mirror, the goal is tightened at large separations by subtracting the contribution of wavefront tilt to the atmospheric structure function. The target structure function, including these two modifications, is shown in Figure 6.

Accuracy in radius of curvature and conic constant, or spherical aberration, are treated as separate requirements. The allowed error in conic constant is 10^{-4} , corresponding to 81 nm peak-to-valley surface spherical aberration at best focus. The telescope is relatively insensitive to errors in radius of curvature, but the null test of the mirror in the lab is very sensitive to radius errors because they affect the distance from the null lens to the mirror.[8] The allowed error is 1 mm.

3. FABRICATION

The casting, generating and early stages of polishing this mirror are described elsewhere.[2,9] We started loose-abrasive grinding in October 1995, polishing in January 1996, and testing at visible wavelength in October 1996. The process was interrupted for six months to generate and polish the rear surface of the second 6.5 m mirror (for the Magellan Telescope), and we completed the MMT primary in October 1997. Figure 2 shows the mirror on the polishing machine.

For loose-abrasive grinding and polishing we use the same stressed lap, comprising a 1.5 m aluminum plate 50 mm thick and 18 moment-generating actuators around the edge of the plate to bend it elastically. Three more actuators apply lifting forces to control polishing pressure and pressure gradients. The polishing surface is 1.2 m in diameter. The bending actuators are

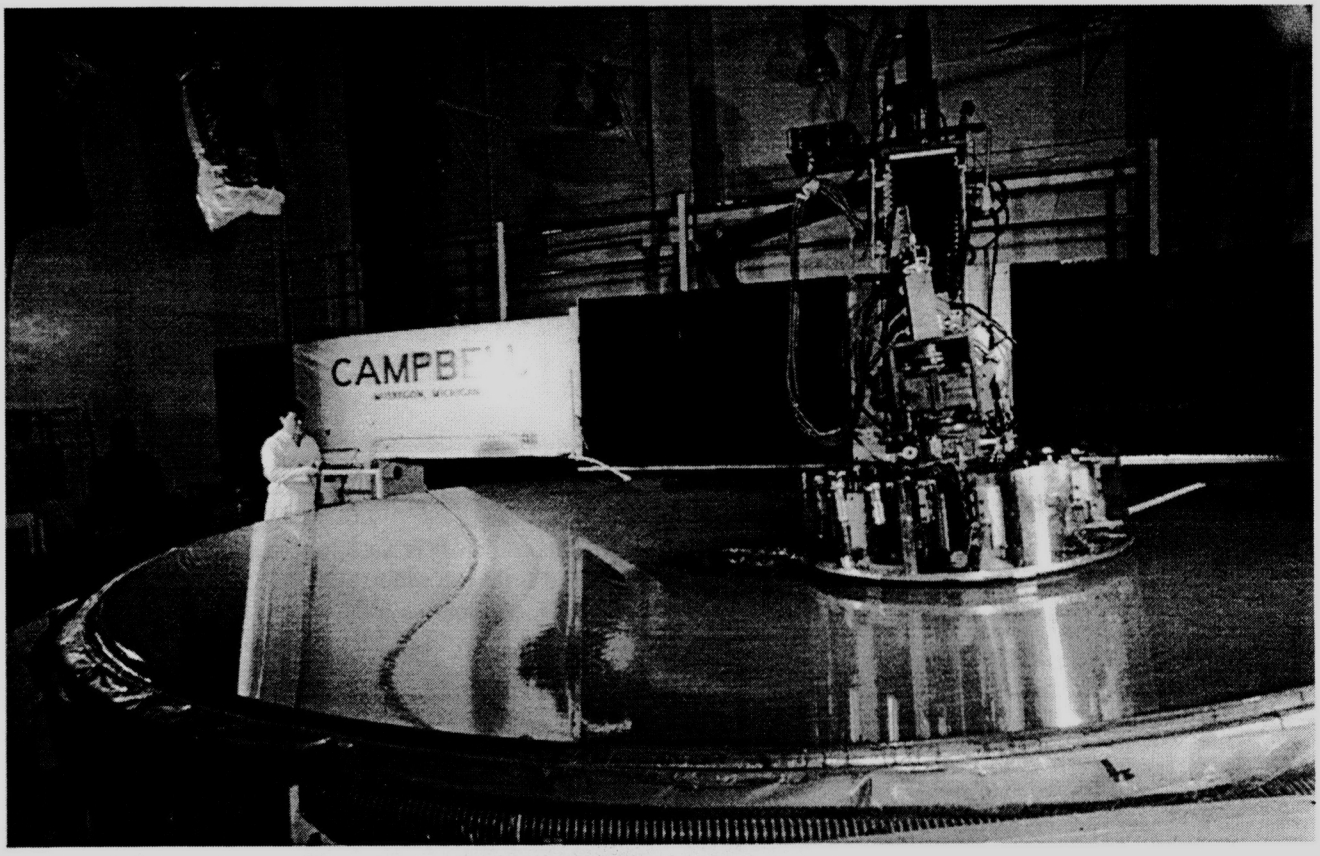

Figure 2. MMT primary mirror being polished.

programmed to make the lap shape match the ideal parabolic mirror surface at all times, while the lifting actuators can be used to vary the pressure according to the current figure error—applying more pressure at the high points—and to balance forces when the lap extends over the edge of the mirror. Figure 3 shows the stressed lap in more detail.

The polishing machine provides dynamic control of the speeds of its three polishing motions (radial, mirror rotation and lap rotation). We generally use the radial motion and lap rotation to control axisymmetric figure errors. Variations in pressure and mirror rotation rate remove non-axisymmetric errors. We control mechanical quilting of the honeycomb structure under polishing pressure by applying an equal air pressure to the inside of the mirror.

In addition to the stressed lap, we used stiff passive tools from 15 to 40 cm in diameter for local figuring. This work included some non-axisymmetric figuring in early stages, but in the final stages it was used to correct relatively narrow symmetric high zones, especially near the outer edge. Short radial strokes were used in order to limit misfit between the lap and the aspheric surface.

4. OPTICAL MEASUREMENT

All lapping operations are guided by phase-shifting interferometry. We use a 10.6 micron interferometer for loose-abrasive grinding and early polishing, and a 531 nm interferometer for the final figuring. Both interferometers are sensitive to surface errors of about $\lambda/100$. Separate IR and visible null lenses correct the 810 micron departure from the best-fitting sphere.

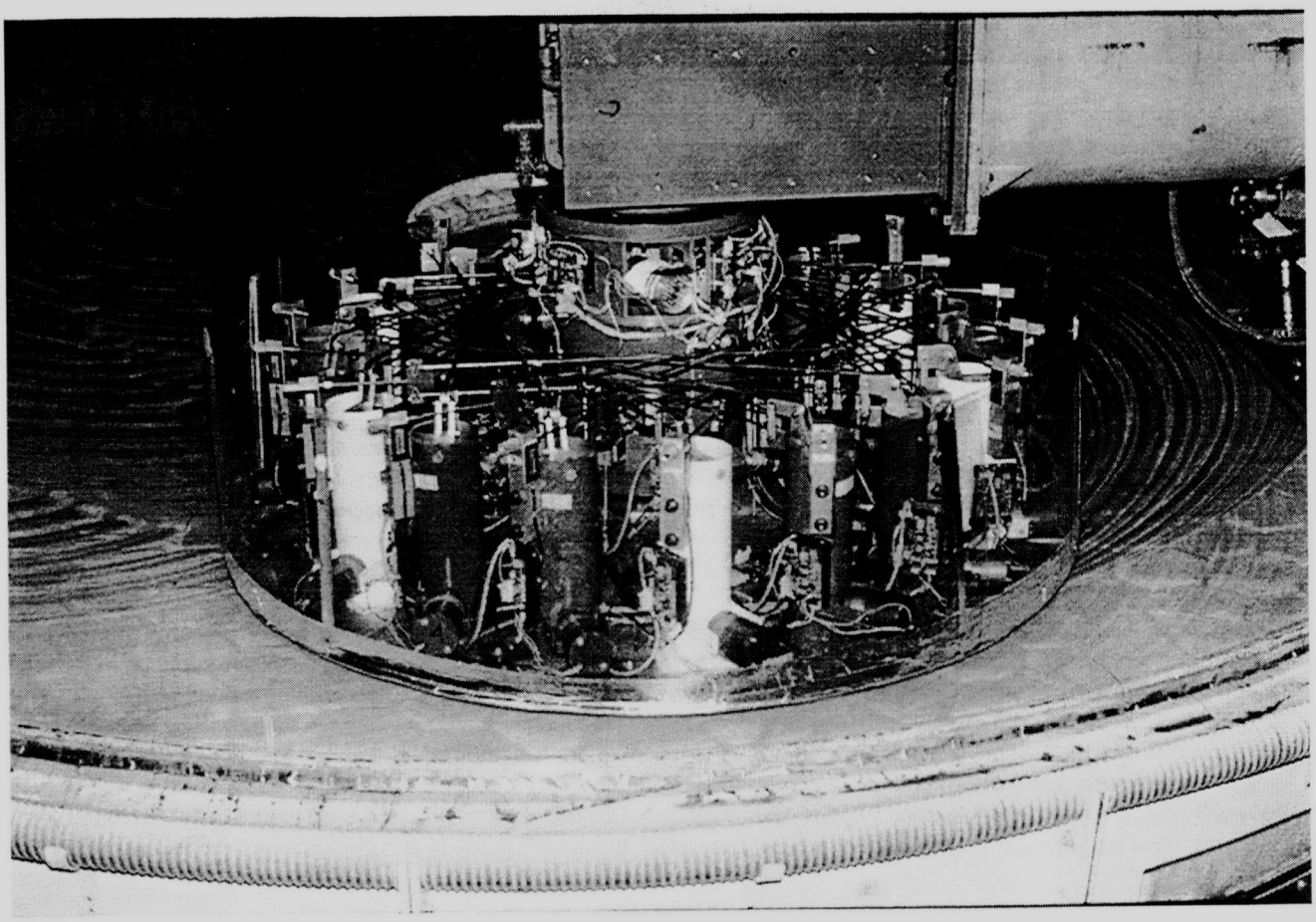

Figure 3. Stressed lap polishing the mirror.

We measured the accuracy of both null lenses using small computer-generated holograms that mimic the ideal primary mirror.[8] Measurement of the visible hologram with the visible null lens revealed a discrepancy of 150 nm of spherical aberration (surface Zernike coefficient), equivalent to 2.7×10^{-4} in conic constant. Among the four independent measurements–IR null lens and hologram, visible null lens and hologram–only the visible null lens disagrees. We have verified the surfaces, radii and spacings of the null lens elements. A possible explanation of the discrepancy that has not been ruled out is a variation of refractive index in the largest element of the null lens, which is 55 mm thick. We are preparing a hologram to measure the wavefront transmitted by this element. We have assumed that the hologram is correct, and figured the mirror using it as the standard for spherical aberration. In the unlikely event that it is incorrect, the spherical aberration could be eliminated in the telescope by a small repositioning of the secondary mirror and instruments.

The interferometer and null lens are positioned as a rigid body with respect to the mirror by visual inspection of the interference fringes. The interferometer is translated to minimize fringes of tilt and focus, and rotated about a point near the mirror's center of curvature to minimize coma. (This positioning is equivalent to finding the portion of the mirror surface that best matches a paraboloid. A separate measurement of radius of curvature verifies that this is the correct paraboloid, and a separate measurement of decenter coma verifies that the axis of this paraboloid is accurately aligned with the mechanical axis of the mirror.) Residual errors of tilt, focus and coma in the surface map are subtracted.

For the final measurements the mirror was allowed to equilibrate thermally for 2 days. We routinely measured glass temperatures at 24 locations inside the honeycomb structure, and found that the mirror became stable and isothermal within 0.2 K peak-to-valley within 24 hours after a polishing run. We monitored support forces at the 104 support locations and found that

they varied by about 5 N rms, probably due to a combination of leakage and friction in the passive hydraulic supports. These force variations are expected to produce astigmatism at a level on the order of 300 nm peak-to-valley surface, and smaller amounts of other flexible bending modes. Variations on this order were observed from day to day. Larger errors in support forces during the generating and loose-abrasive grinding stages led to about 1 micron peak-to-valley astigmatism present in the polished surface at the time of the first visible measurements. We decided to correct this with the active supports in the telescope rather than by polishing it out. These amplitudes of flexible bending modes have no effect on telescope performance, as they will be controlled by the active support system.[10]

5. RESULTS

5.1 Acquisition and processing of data

We present the final results in the form of surface contour maps and synthetic interference patterns, structure function, and point-spread functions. The data presented here are based on an average of 46 phase maps. The noise in an individual map, caused primarily by seeing, averages about 50 nm rms surface error and shows little or no correlation between maps. The noise in the average should be less than 10 nm rms. The aberrations of tilt, focus and coma, which result from slight misalignment of the interferometer with respect to the optical axis of the mirror, have been subtracted.

The raw data contain variable amounts of astigmatism averaging about 1 micron peak-to-valley, probably related to variations in support forces. This has been subtracted from the maps, as it is easily corrected with the active supports in the telescope. These data are shown in Figure 4. In addition to astigmatism, several other flexible bending modes with small amplitudes are caused primarily by variations in support forces, and their amplitudes in the telescope will be determined more by support forces than by the relaxed mirror figure. Subsequent optimization of forces with the mirror on its active telescope supports confirmed that these aberrations are controllable with modest forces.[10] Similarly, spherical aberration will be determined by the spacing of the telescope's optics. Data with these additional aberrations removed (listed in Table 1) are shown in Figure 5. This best represents the potential performance of the mirror and is used for the diffraction calculations.

Table 1: Aberrations subtracted from final map

aberration	Zernike coefficient (nm of surface)
3rd-order astigmatism	530
spherical	14
trefoil	32
5th-order astigmatism	55

5.2 Mirror figure and structure function

Figures 4 and 5 are gray-scale surface maps and synthetic interference patterns. The full measured aperture (shown in the figures) covers a diameter of 6.49 m with a resolution of 197×231 pixels. The overall surface error is 35 nm rms with astigmatism subtracted, and 26 nm rms with the three additional aberrations subtracted. Figure 6 shows the wavefront structure function, calculated over a clear aperture with outer diameter 6.435 m and inner diameter 1.235 m. The inner diameter corresponds to the obscuration of the f/9 secondary mirror, the smallest obscuration for visible wavelength observations.

5.3 Diffraction calculations

Diffraction calculations were made from the map of Figure 5, using the same clear aperture used for the structure function. The calculation covers a 4 arcsecond field, but only the central 0.5 arcsecond square is displayed. Figure 7 shows the

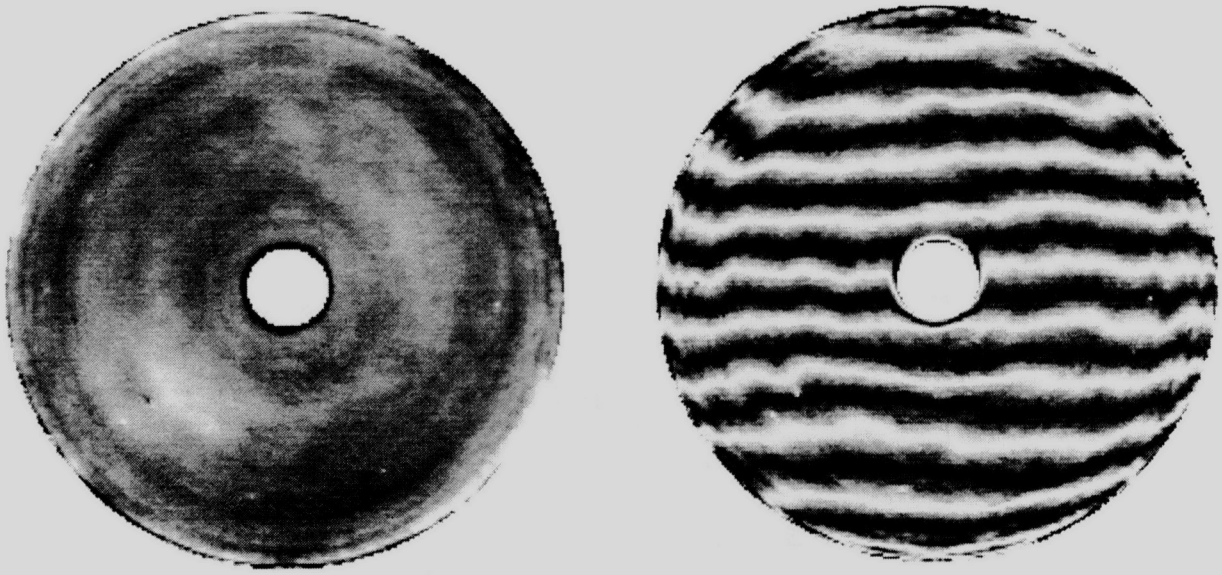

Figure 4. Gray-scale map of the mirror surface with astigmatism subtracted (left) and synthetic interference pattern (right). The rms surface error is 35 nm. The gray scale covers ±100 nm of surface. The interference pattern is calculated for a wavelength of 531 nm.

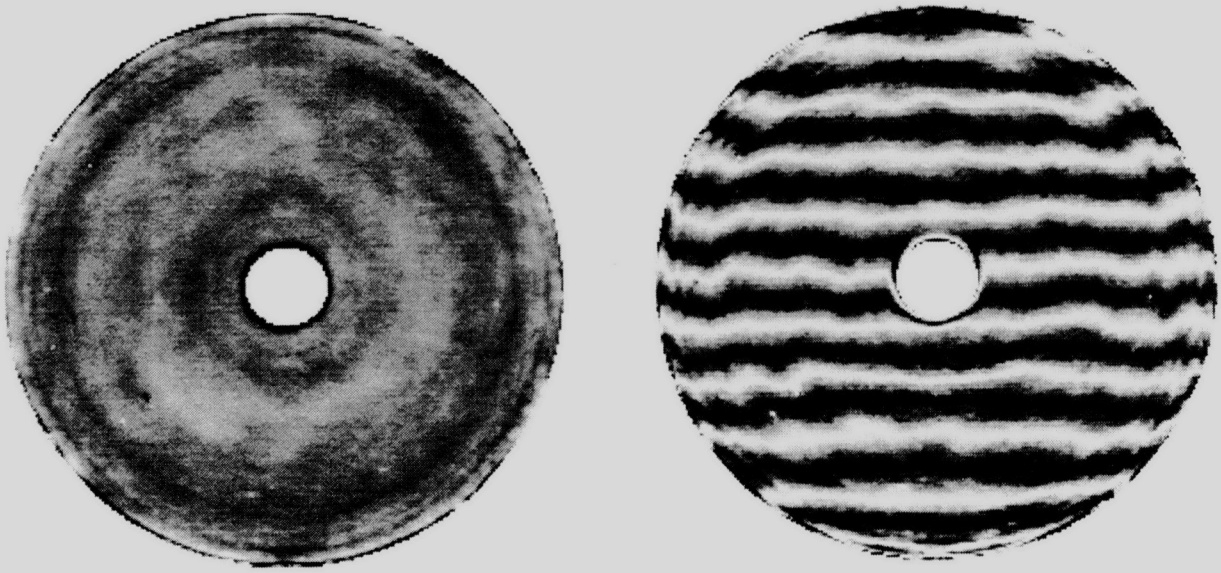

Figure 5. Same as Figure 4 except that three additional aberrations have been subtracted. The rms surface error is 26 nm.

point-spread functions of the actual mirror and a perfect mirror. Figure 8 shows encircled energy diagrams for the actual mirror in seeing of 0, 0.25 and 0.5 arcsecond. In perfect seeing the mirror focuses 80% of the light at 500 nm into a 0.13 arcsecond diameter. Figure 9 shows the central intensity ratio, defined as the ratio of central intensity for the actual mirror plus atmosphere to that for a perfect mirror plus atmosphere, as a function of seeing quality.

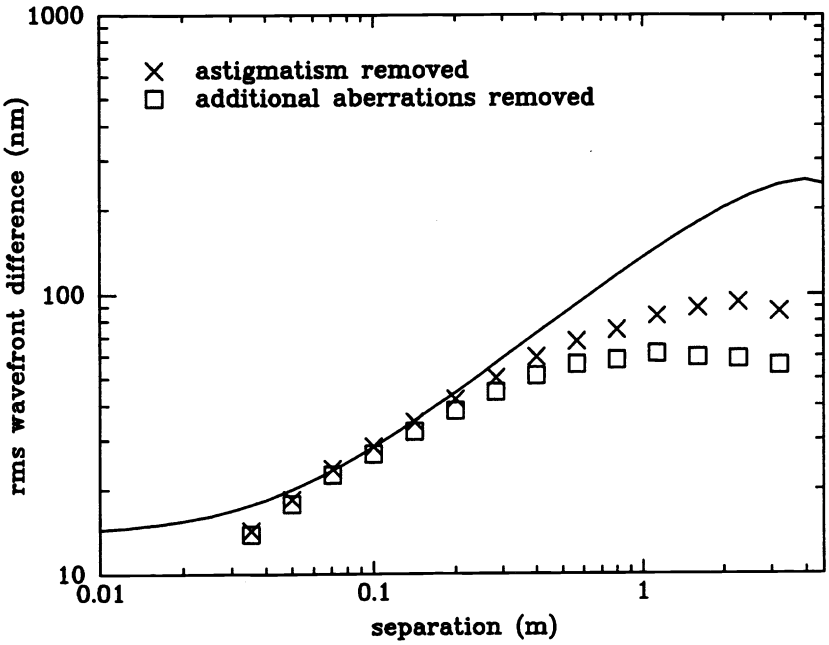

Figure 6. Square root of the wavefront structure function for the mirror with astigmatism subtracted and with three additional aberrations subtracted. The curve is the goal.

Figure 7. Point spread functions at 0.5 micron for the actual mirror of Figure 5 (left) and a perfect mirror (right). The images are separated by 0.5 arcsecond.

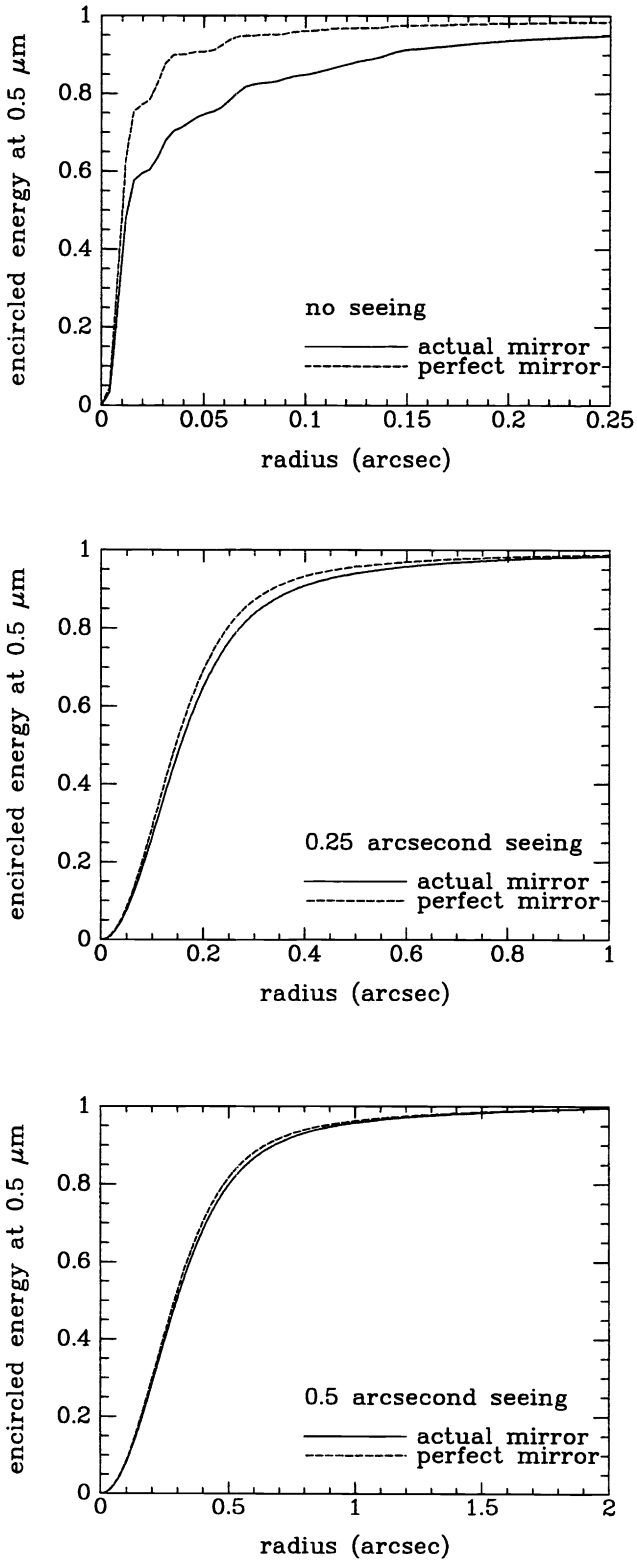

Figure 8. Encircled energy diagrams for the mirror of Figure 5 and a perfect mirror, in various seeing conditions.

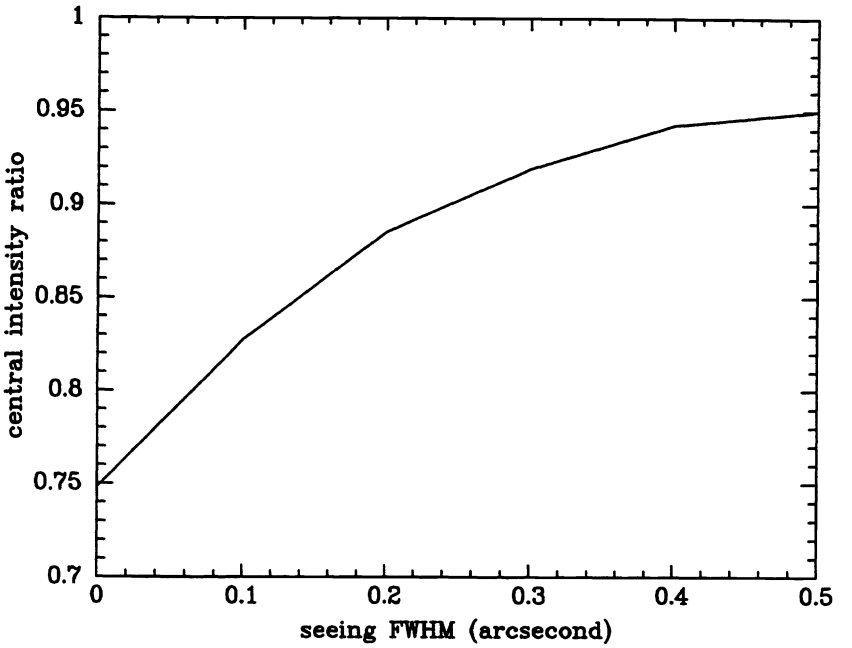

Figure 9. Central intensity ratio as a function of seeing quality. The central intensity ratio is defined as the ratio of central intensity for the actual mirror plus atmosphere to that for a perfect mirror plus atmosphere.

5.4 Subaperture measurements

A set of subaperture measurements was made as a check on small-scale structure that might not be completely resolved in the full-aperture maps. These maps, shown in Figure 10, have 2.9 times the resolution of the full-aperture maps. In subaperture maps one cannot completely distinguish alignment aberrations (those caused by slight misalignment of the interferometer) from large-scale figure errors. We have subtracted tilt, focus, astigmatism and coma, fit in local coordinates for each subaperture. While this correction removes more than alignment errors, all errors removed are already well measured in the full-aperture map, and are easily controlled with the active supports.

The subaperture structure functions are shown in Figure 11. They show only a slight increase in structure at small scales relative to the full-aperture structure function. Subaperture C contains large-scale structure that is inconsistent with the full-aperture map, and may be due to temperature inhomogeneity at the time of the subaperture measurement.

6. CONCLUSION

We have figured the MMT primary mirror to an accuracy of 26 nm rms surface error (excluding certain flexible bending modes), with 80% of the light at 500 nm focussed within a 0.13 arcsecond diameter. The mirror will make a negligible contribution to image degradation in the best seeing at Mt. Hopkins. With the successful completion of the MMT primary, the Mirror Lab moves on to two more 6.5 m f/1.25 mirrors for the Magellan Telescopes in Chile, and two 8.4 m f/1.14 mirrors for the Large Binocular Telescope in Arizona.

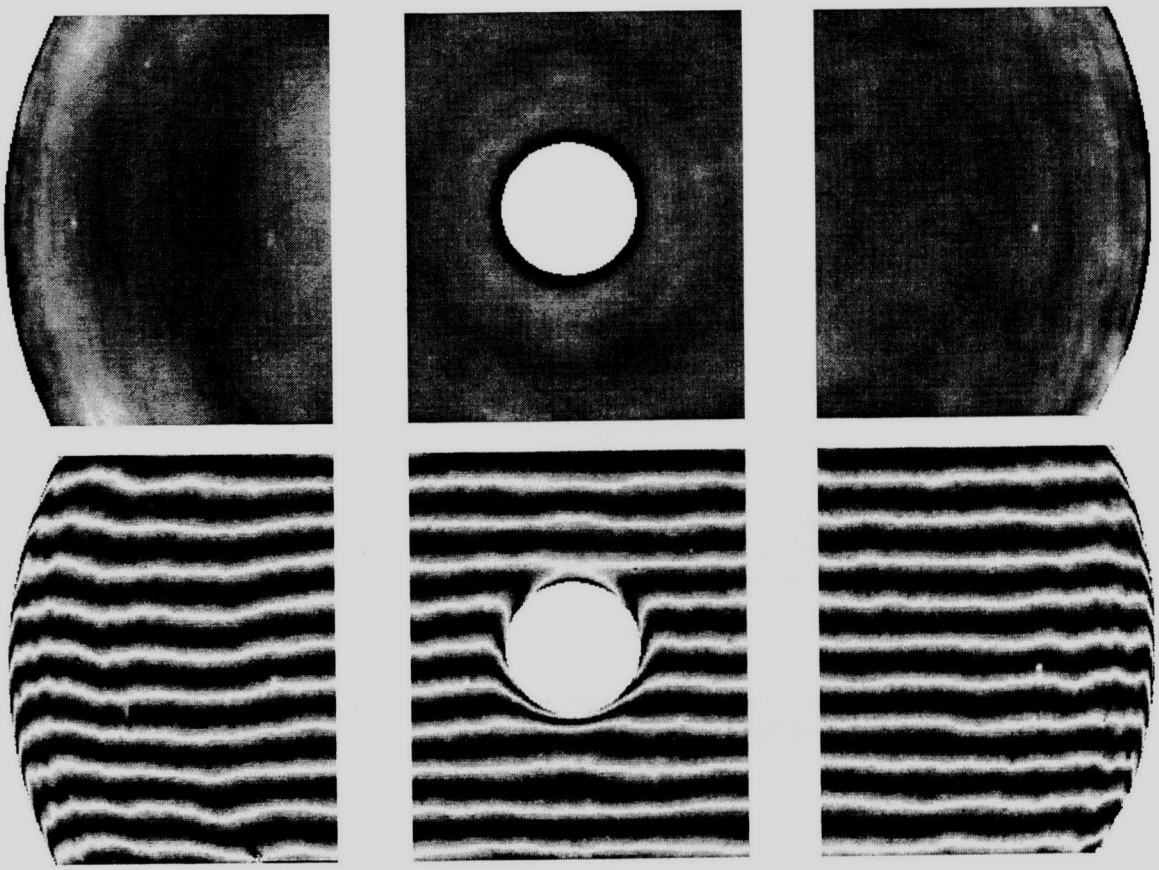

Figure 10. Gray-scale contour maps and synthetic interference patterns for three subapertures (A, B and C from right to left) across the diameter of the mirror. The gray scale covers ±100 nm of surface. The interference pattern is calculated for a wavelength of 531 nm. The displays extend to the edges of the polished surface.

7. REFERENCES

1. S. C. West, S. Callahan, F. H. Chaffee, W. B. Davison, S. T. DeRigne, D. G. Fabricant, C. B. Foltz, J. M. Hill, R. H. Nagel, A. D. Poyner, J. T. Williams, "Toward first light for the 6.5-m MMT telescope", in *Optical Telescopes of Today and Tomorrow: Following in the Direction of Tycho Brahe*, Arne Ardeberg, Editor, Proc. SPIE 2871, p. 38 (1997).

2. B. H. Olbert, J. R. P. Angel, J. M. Hill, S. F. Hinman, "Casting 6.5-meter mirrors for the MMT conversion and Magellan", in *Advanced Technology Optical Telescopes V*, Larry M. Stepp, Editor, Proc. SPIE 2199, p. 144 (1994).

3. M. Johns, "Magellan 6.5-m Telescopes Project: status report", in *Optical Telescopes of Today and Tomorrow: Following in the Direction of Tycho Brahe*, Arne Ardeberg, Editor, Proc. SPIE 2871, p. 49 (1997).

4. J. M. Hill, "Large Binocular Telescope Project", in *Optical Telescopes of Today and Tomorrow: Following in the Direction of Tycho Brahe*, Arne Ardeberg, Editor, Proc. SPIE 2871, p. 57 (1997).

5. H. M. Martin, D. S. Anderson, J. R. P. Angel, R. H. Nagel, S. C. West, R. S. Young, "Progress in the stressed-lap polishing of a 1.8-m f/1 mirror", in *Advanced Technology Optical Telescopes IV*, Lawrence D. Barr, Editor, Proc. SPIE 1236, p. 682 (1990).

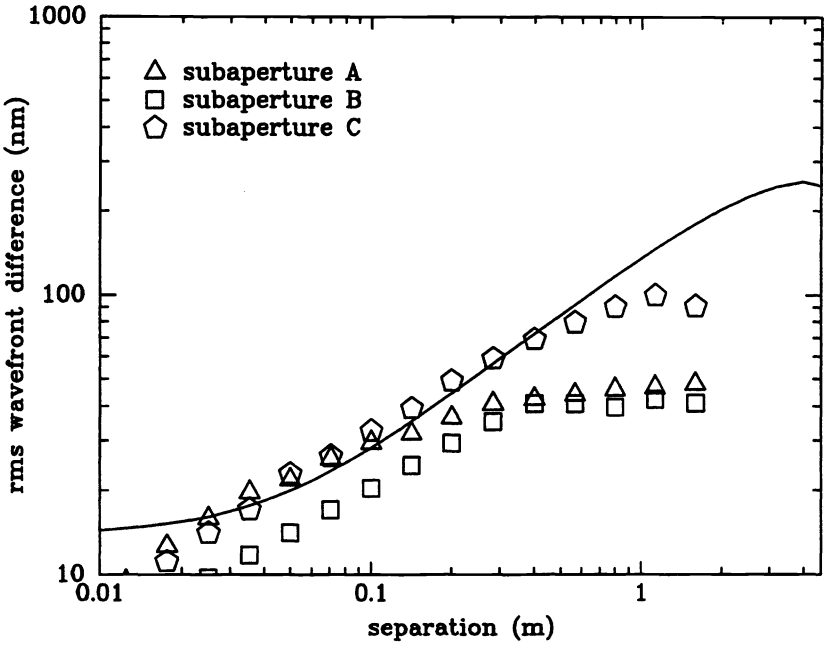

Figure 11. Square root of the wavefront structure function for the subaperture measurements shown in Figure 10. Only data within the clear aperture defined in Section 5.2 are used. The curve is the goal for the average structure function over the mirror.

6. H. M. Martin, D. S. Anderson, J. R. P. Angel, J. H. Burge, W. B. Davison, S. T. DeRigne, B. B. Hille, D. A. Ketelsen, W. C. Kittrell, R. McMillan, R. H. Nagel, T. J. Trebisky, S. C. West, R. S. Young, "Stressed-Lap Polishing of 1.8-m f/1 and 3.5-m f/1.5 Primary Mirrors", in *Proc. ESO Conference on Progress in Telescope and Instrumentation Technologies*, M.-H. Ulrich, Editor, p. 169 (1992).

7. S. C. West, H. M. Martin, R. H. Nagel, R. S. Young, W. B. Davison, T. J. Trebisky, S. T. DeRigne, B. B. Hille, "Practical Design and Performance of the Stressed-Lap Polishing Tool", *Applied Optics* 33, p. 8094 (1994).

8. J. H. Burge, D. S. Anderson, D. A. Ketelsen, S. C. West, "Null test optics for the MMT and Magellan 6.5-m f/1.25 primary mirrors", in *Advanced Technology Optical Telescopes V*, Larry M. Stepp, Editor, Proc. SPIE 2199, p. 658 (1994).

9. H. M. Martin, J. H. Burge, D. A. Ketelsen, S. C. West, "Fabrication of the 6.5 m primary mirror for the Multiple Mirror Telescope Conversion", in *Optical Telescopes of Today and Tomorrow: Following in the Direction of Tycho Brahe*, Arne Ardeberg, Editor, Proc. SPIE 2871, p. 399 (1997).

10. H. M. Martin, W. B. Davison, S. T. DeRigne, G. Parodi, T. J. Trebisky, S. C. West, "Active supports and force optimization for the MMT primary mirror", in these proceedings.